Polymer Chemistry

ROYAL SOCIETY OF CHEMISTRY

PAPER

View Article Online
View Journal | View Issue

Check for updates

Cite this: *Polym. Chem.*, 2023, **14**, 1965

Amphiphilic tetra-PCL-*b*-PEG star block copolymers using benzoxazinone-based linking groups†

Carolin Bunk, [a,b] Hartmut Komber, [a] Michael Lang, *[a] Nora Fribiczer,[c] Martin Geisler, [a] Petr Formanek, [a] Lothar Jakisch,[a] Sebastian Seiffert, [c] Brigitte Voit [a,b] and Frank Böhme *[a]

Received 25th January 2023,
Accepted 27th March 2023

DOI: 10.1039/d3py00078h

rsc.li/polymers

In this study, two well-defined amphiphilic tetra-arm star block copolymers with a poly(ε-caprolactone) (ε-CL) core and poly(ethylene glycol) (PEG) arms with different length (800 g mol^{-1} and 2100 g mol^{-1}) were prepared by a hetero-complementary linking reaction and studied in detail. A pentaerythritol core was used as an initiator for the ring-opening polymerization (ROP) of ε-CL, generating a hydroxy-terminated tetra-arm star polymer (tetra-PCL–OH) with controlled molar mass (M_n ~ 10 kg mol^{-1}) and low dispersity ($Đ$ < 1.1). After end group esterfication with 2-(4-nitrophenyl)-4-oxo-4*H*-benzo[*d*][1,3]oxazine-7-carboxylic acid chloride, linear hydrophilic PEG was attached to the respective tetra-PCL to obtain tetra-PCL-*b*-PEG star block copolymers. The behavior of the two amphiphilic block copolymers was studied in water by a combination of variable-temperature ^{1}H NMR spectroscopy, DLS, DSC and TEM measurements. In the case of longer PEG arms, spherical micelles form at elevated temperatures and remain stable at room temperature over days. Transmission electron microscopy indicates a possible slow morphology change of spherical micelles into long cylindrical micelles after one week. Suspensions of the star block copolymers with the short PEG arms in water remain cloudy, in contrast to the star block copolymers with long arms.

Introduction

Star block copolymers consist of chemically distinct polymer segments (AB-type arms or A-type and B-type arms) connected by a central branching point called the core.[1,2] They represent an attractive class of branched polymers which differ distinctly from their linear analogs in terms of a reduced hydrodynamic volume, lower dispersity ($Đ$), and high functionality with the same synthesis strategy, molar mass and composition.[2–5] There are two main strategies for producing this type of polymer: "arm-first" and "core-first" where either the block-copolymer arms or the central homopolymer star are synthesized first. For the latter strategy, one considers in general that the second block of the arms is polymerized in a subsequent step, while the "grafting-onto" variant of the core-first strategy describes the subsequent attachment of independently functionalized and synthesized polymers, *e.g.* by "click" chemistry or Steglich esterification.[2,6–10] This last approach allows designing star block copolymers with the highest structural control. Star block copolymers with both hydrophilic and hydrophobic components, such as poly(ethylene glycol) (PEG), the most widely used biocompatible polymer for biological applications, and poly(ε-caprolactone) (PCL), a biodegradable and non-toxic industrial polyester, have proven to be useful materials for biomedical applications.[11–14] This is due to the amphiphilic nature of PCL-*b*-PEG copolymers, manifested in their tendency to form self-assembling micelles, vesicles, or gels.[3,15–21]

Micelles prepared from PCL-*b*-PEG star block copolymers were frequently studied (see ESI Table S3†), since the micelle stability of stars is increased over their linear counterparts.[3,16] As shown in Table S3,† all strategies have been used to prepare a broad variety of star polymers with different cores and functionalities providing molar masses from 10 kg mol^{-1} to beyond 200 kg mol^{-1}. High molecular weight stars with PCL as the outer block ("tail") first form micelles and then may gel upon increasing polymer volume fraction in water,[16] while stars with PEG tails do not gel upon micro-phase separation in

[a]*Leibniz-Institut für Polymerforschung Dresden e.V., Hohe Straße 6, Dresden, Germany. E-mail: boehme@ipfdd.de, lang@ipfdd.de*
[b]*Organische Chemie der Polymere, Technische Universität Dresden, 01062 Dresden, Germany*
[c]*Department Chemie, Johannes Gutenberg-Universität Mainz, Duesbergweg 10-14, 55128 Mainz, Germany*

†Electronic supplementary information (ESI) available: DLS of **6a** and **6b**, NMR spectra of **1**, **3**, **5**, **6**, **7**, and **8**, temperature dependent NMR spectra of **6a** and **6b**, MALDI-TOF and MD-SEC of **1**, **3**, **5**, and **6**. See DOI: https://doi.org/10.1039/d3py00078h

water. A crucial point of these materials is that both polymers crystallize at similar temperatures, such that structure formation may depend on solvent quality or additional details of the sample preparation.[22] This difficulty is partially visible in the micellization data summarized in ESI Tables S3 and S4† where significant changes in micelle size or critical micelle concentration were observed for copolymers of similar architecture, molar mass and composition. Our interest in tetra-PCL-*b*-PEG micelles stems from investigations on model amphiphilic co-networks based on tetra-arm PEG and PCL star polymers.[23–25] Here, soluble amphiphilic star block copolymers containing the same building blocks are needed to structure the material prior to network formation.

In the present work, such star block copolymers were synthesized in a similar manner as the co-networks by grafting amino-terminated linear PEGs of different molar mass onto benzoxazinone-terminated tetra-arm PCL (see Scheme 1). By using the bi-functional benzoxazinone-based coupling agent **2**, which reacts hetero-complementarily with hydroxy and amino groups under mild conditions without any by-products,[26–28] uniform star block copolymers can be prepared. Particular attention was paid to the defined structure of the tetra-PCL–OH core **1**, its quantitative benzoxazinone functionalization (**3**), and their subsequent complete reaction with amino-terminated PEG **5** to form uniform tetra-PCL-*b*-PEG star block copolymers **6**. Furthermore, the influence of PEG chain length on the behavior of the star block copolymers in aqueous medium and on the formation and stability of micellar structures was studied in detail.

Experimental section

Materials

All chemicals and solvents (analytical grade) were obtained from Sigma-Aldrich and used as received unless otherwise specified. Methoxy poly(ethylene glycol) (MeO–PEG–OH) (M_n = 2100 g mol^{-1}) was obtained from JenKem Technology (USA) and precipitated twice from THF in cold diethyl ether. Mono-amino-terminated MeO–PEG (MeO–PEG–NH_2, **5a**, M_n = 822 g mol^{-1}) was obtained from Iris Biotech (Germany). ε-Caprolactone (ε-CL) was dried under reduced pressure over CaH_2 for at least 12 hours, then purified by vacuum distillation and stored under nitrogen atmosphere. Tin(II)-2-ethylhexanoate ($Sn(oct)_2$) was purified by vacuum distillation and stored under nitrogen atmosphere. 2-(4-Nitrophenyl)-4-oxo-4*H*-benzo[*d*][1,3]oxazine-7-carboxylic acid chloride **2** was synthesized as described earlier.[27–29]

Synthetic procedures

Tetra-PCL–OH (1). Following Jakisch *et al.*, two batches (**a**, **b**) of **1** were prepared by bulk polymerization of ε-CL with pentaerythritol as initiator using $Sn(oct)_2$ as catalyst.[26] The target M_n of 10 kg mol^{-1} was adjusted by the ε-CL : $Sn(oct)_2$: pentaerythritol molar ratio of 87 : 0.1 : 1. The synthesis was carried out as follows: first, 136 mg of pentaerythritol and 9.92 g of ε-CL were added to a Schlenk flask at room temperature under nitrogen. The dispersion was stirred at 120 °C for 30 min to obtain a homogeneous mixture. The reaction mixture was cooled to 80 °C and the polymerization was started by injecting the catalyst ($Sn(oct)_2$, 0.2 mL of 0.5 M dry toluene solution) under nitrogen. After 2 h, the reaction temperature was increased to 100 °C for another 6 h. Then, the very viscous reaction mixture was cooled to room temperature to stop the bulk polymerization. The polymer was purified by precipitation from a concentrated CH_2Cl_2 solution into a 10-fold amount of cold methanol. After filtration and drying in vacuum, a powdery product of **1** was obtained.

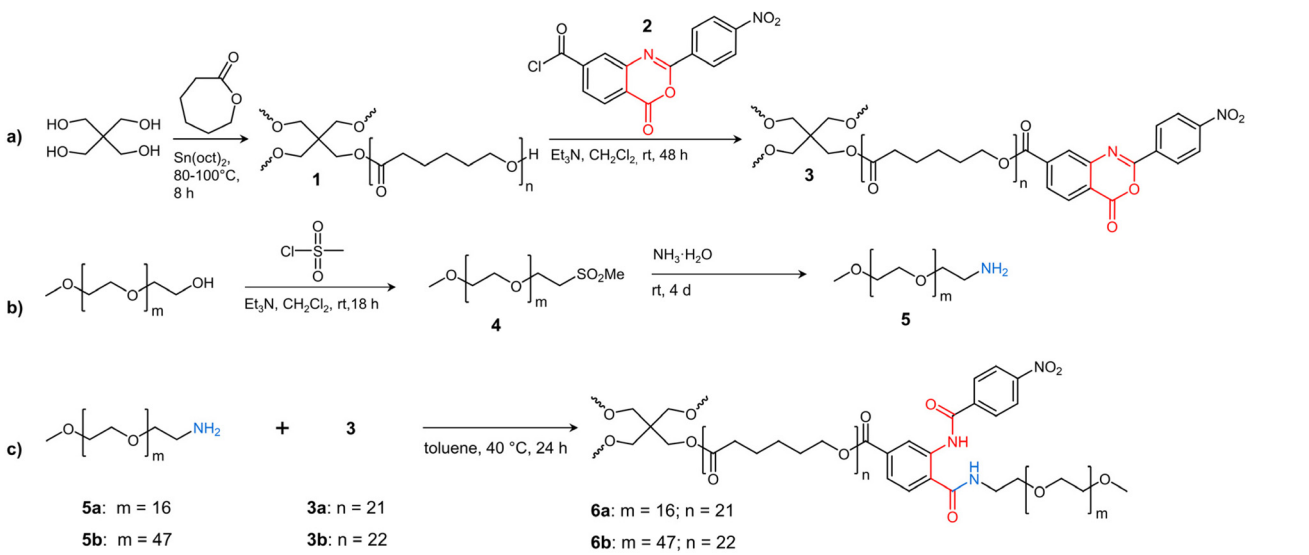

Scheme 1 Synthesis of (a) 2-(4-nitrophenyl)-benzoxazinone-terminated tetra-PCL star polymer **3**, (b) MeO–PEG–NH_2 **5**, and (c) amphiphilic tetra-PCL-*b*-PEG star block copolymer **6**.

^{1}H NMR ($CDCl_3$): δ 4.11 (s; $CH_{2,core}$), 4.06 (t, 6.7 Hz; $CH_2OC(O)$), 3.65 (t, 6.5 Hz; CH_2OH), 2.30 (t, 7.6 Hz; $CH_2C(O)O$), 1.7–1.6 ($CH_2CH_2CH_2$), 1.38 ppm (m; $CH_2CH_2CH_2$).

^{13}C NMR ($CDCl_3$): δ 173.3 (C=O), 172.7 (C=O next to core), 64.0 ($CH_2OC(O)$), 62.4 (CH_2OH), 61.9 ($CH_{2,core}$), 41.9 (C_{core}), 34.0 ($CH_2C(O)O$), 32.2 (CH_2CH_2OH), 28.2 ($CH_2CH_2OC(O)$), 25.4 ($CH_2CH_2C(O)O$), 24.4 ppm ($CH_2CH_2CH_2$).

2-(4-Nitrophenyl)-benzoxazinone-terminated tetra-PCL (3). Compound **3** was prepared as described earlier[26] by conversion of **1** with 2-(4-nitrophenyl)-4-oxo-4*H*-benzo[*d*][1,3]oxazine-7-carboxylic acid chloride **2** (Scheme 1a). An amount of 0.5 mmol of **1** was dissolved in dry CH_2Cl_2 (30 mL). Then, 4.5 mmol (0.62 mL) of triethylamine and 4 mmol of previously dissolved **2** in dry CH_2Cl_2 (15 mL) were slowly added to the solution at room temperature under nitrogen using a syringe. The reaction mixture was stirred for 48 h, the insoluble salt (triethylammonium chloride) was removed by filtration and **3** was obtained by precipitation in cold methanol. **3** was prepared in two batches (**a**, **b**) used for the synthesis of **6a** and **6b**.

^{1}H NMR ($CDCl_3$): δ 8.52 (d, 8.8 Hz; 19), 8.39 (s; 11), 8.38 (d, 8.8 Hz; 20), 8.34 (d, 8.2 Hz; 14), 8.20 (d, 8.2 Hz; 15), 4.41 (t, 6.7 Hz; 8 next to C_9), 4.10 (s; 2), 4.06 (t, 6.7 Hz; 8), 2.35 (t, 7.4 Hz; 4 next to C_9), 2.30 (t, 7.4 Hz; 4), 1.85 (m; 7 next to C_9), 1.73 (m; 5 next to C_9), 1.7–1.6 (5, 7), 1.52 (m; 6 next to C_9), 1.38 ppm (m; 6).

^{13}C NMR ($CDCl_3$): δ 173.4 (3), 172.8 (3 next to core), 164.7 (9), 158.0 (16), 155.6 (17), 150.3 (21), 146.3 (12), 138.1 (10), 135.5 (18), 129.4 (15), 129.3 (19), 129.0 (14), 128.9 (11), 123.9 (20), 120.0 (13), 65.8 (8 next to C_9), 64.1 (8), 61.9 (2), 42.0 (1), 34.1 (4), 28.3 (7), 25.5 (5), 24.5 ppm (6).

MeO–PEG–NH$_2$ (5b). Compound **5b** was synthesized in two steps by adapting a previously reported procedure (Scheme 1b).[30] In the first step, MeO–PEG–OH (M_n = 2100 g mol^{-1}, m = 47) was converted with mesylchloride to MeO–PEG–OMs intermediate (**4**). The resulting mesyl groups were subsequently converted into amino groups by reaction with aqueous ammonia. Briefly, an amount of 1 mmol of MeO–PEG–OH, 8.5 mmol of triethylamine and 8 mmol of mesylchloride were dissolved in anhydrous CH_2Cl_2 (50.0 mL) and stirred overnight. The solution was filtered and the solvent was evaporated. The polymer was dissolved in THF and poured into a large excess of cold diethyl ether. The precipitated white solid of **4** was isolated by filtration and dried under vacuum at 40 °C. The purified **4** with terminal mesyl groups was dissolved in 28 wt% aqueous ammonia solution (100 mL). The reaction mixture was left with stirring for 5 days at room temperature. The ammonia was allowed to evaporate over night after NaOH (5 M) was added dropwise until the pH reached 13. After the product was extracted 3 times with CH_2Cl_2 and washed with saturated sodium chloride solution, drying over anhydrous $MgSO_4$ followed. The crude product was precipitated into a 10-fold amount of cold diethyl ether. The precipitate was filtered and dried under vacuum at 40 °C.

^{1}H NMR ($CDCl_3$): δ 3.62 (s; c), 3.48 (m; b), 3.35 (s; d), 2.84 (t, 5.3 Hz; a), 1.8 ppm (v br; NH_2).

^{13}C NMR ($CDCl_3$): δ 73.3 (b), 71.5, 70.5, 70.2 (all c), 58.9 (d), 41.7 ppm (a).

Tetra-PCL-*b*-PEG star block copolymer (6). Star block copolymer **6a** and **6b** with two PEG blocks of different lengths were prepared by the hetero-complementary amine–benzoxazinone reaction of **3** with **5** in toluene (Scheme 1c). As an example, the synthesis of **6b** was carried out as follows: an amount of 0.1 mmol of **3a** was dissolved in anhydrous toluene (10 mL). Then, 0.45 mmol of **5b** were added to the solution and stirred 24 h under nitrogen at 40 °C. The solvent was removed by evaporation and the obtained slightly yellowish powder was dispersed in water. The residue of **5b** was then extracted from the solid by centrifugation at 20 °C for 20 minutes at 20 400*g*. The supernatant was then removed, fresh water added, and centrifuged again. This procedure was carried out 4 times. The purified powder was then freeze-dried to give **6b**.

^{1}H NMR (**6b**, $CDCl_3$). δ 12.62 (s; Ph–N*H*–CO–Ph), 9.41 (s; 11), 8.36 (d, 8.8 Hz; 20), 8.21 (d, 8.8 Hz; 19), 7.82 (d, 8.2 Hz; 15), 7.75 (d, 8.2 Hz; 14), 7.36 (t, 5.4 Hz; CH_2–N*H*–CO–Ph), 4.41 (t, 6.7 Hz; 8 next to C_9), 4.10 (s; 2), 4.05 (t, 6.7 Hz; 8), 3.70–3.50 (a, b, c), 3.37 (s; d), 2.34 (t, 7.4 Hz; 4 next to C_9), 2.30 (t, 7.4 Hz; 4), 1.83 (m; 7 next to C_9), 1.72 (m; 5 next to C_9), 1.7–1.6 (5, 7), 1.50 (m; 6 next to C_9), 1.38 ppm (m; 6).

^{13}C NMR (**6b**, $CDCl_3$): δ 173.2 (3), 172.5 (3 next to core), 168.3 (16), 165.3 (9), 163.0 (17), 149.6 (21), 140.0 (18), 139.5 (12), 133.9 (10), 128.4 (19), 127.3 (14), 124.0 (15), 123.7 (20), 123.2 (13), 121.8 (11), 71.7 (c next to C_d), 70.5–69.0 (b, c), 65.1 (8 next to C9), 63.8 (8), 61.7 (2), 58.7 (d), 41.8 (1), 39.9 (a), 33.9 (4), 28.1 (7), 25.3 (5), 24.3 ppm (6).

Model reaction with pentaerythritol. As model compounds for NMR signal assignments, mixtures of alkyl ester- and benzoxazinone-substituted pentaerythritol (**7**, **8**) were obtained by subsequent reaction of pentaerythritol with lauryl chloride and compound **2** (Scheme 2). First, an excess of pentaerythritol was reacted in a non-stoichiometric ratio with lauryl chloride in presence of triethylamine as acid scavenger overnight at room temperature in THF. The precipitate was filtered off, the

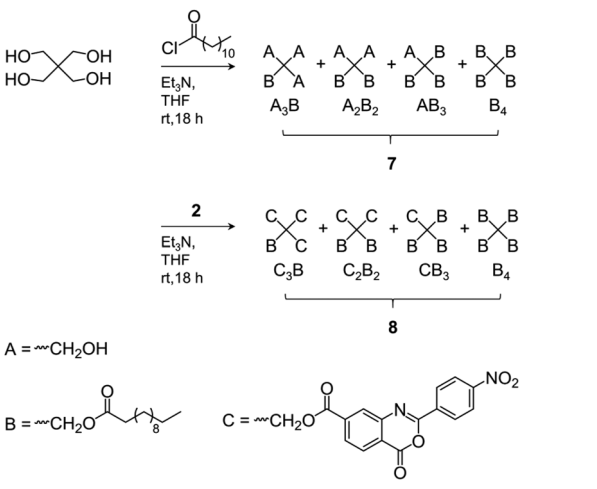

Scheme 2 Synthesis of alkyl ester- (**7**) and benzoxazinone/alkyl ester-substituted (**8**) pentaerythritol mixtures as model compounds for NMR signal assignments.

product was washed several times with water and dried under vacuum to give **7** consisting of a mixture of partially (A_3B, A_2B_2, AB_3) and completely (B_4) esterified pentaerythritol. Subsequently, the mixture **7** was reacted with a twofold excess of compound **2** in presence of triethylamine in THF. After stirring the reaction mixture over night, the insoluble salt was removed by filtration and the crude product mixture **8** (C_3B, C_2B_2, CB_3 and B_4) was purified by precipitation into a 10-fold amount of cold methanol. The precipitate was filtered and dried under vacuum at 40 °C.

Methods

NMR spectroscopy. ^{1}H (500.13 MHz) and ^{13}C (125.76 MHz) NMR spectra were recorded using an Avance III 500 spectrometer (Bruker Biospin). $CDCl_3$ ($\delta(^1H)$ = 7.26 ppm; $\delta(^{13}C)$ = 77.0 ppm) and D_2O ($\delta(^1H)$ = 4.79 ppm) were used as solvent, lock, and internal standard. Sample temperature was kept constant at 30 °C ± 0.5 K unless otherwise specified. For temperature dependent measurements, powdered **6** was finely dispersed in D_2O and immediately transferred in tubes to the spectrometer for the measurements. The sedimentation during the measurements was slow and was assumed not to influence the results. The spectra were referenced on the $H_{5,7}$ signal of PCL ($\delta(^1H)$ = 1.55 ppm).

MD-SEC. Multidetection-hyphenated size exclusion chromatography (MD-SEC) of **1**, **3**, **6a** and **6b** was performed in THF with a flow rate of 1 mL min^{-1} using an Agilent degasser, an isocratic pump and an autosampler (series 1100/1200). Star polymers **1** and **3** were separated with 2× Agilent SEC columns PLgel MIXED-C. Star block copolymers **6a** and **6b** were separated with coupled Shodex SEC columns KF-802 and KF-803. The detection system downstream was comprised of a Wyatt multiangle light scattering detector (MALS) HELEOS® II, a viscometric detector Viscostar® III and a differential refractometer Optilab® T-rEX. The refractive index increment of the samples **3** and **6a**, **6b** in THF was determined in batch to dn/dc = 0.0957 ± 0.0016 mL g^{-1}. For **1**, a dn/dc = 0.072 ± 0.003 mL g^{-1} was used as reported in the literature for PCL in THF.[31,32] MD-SEC of **5a** and **5b** was performed using an aqueous solution containing 0.01 M NaH_2PO_4 (pH = 7) and 0.2 M $NaPO_3$ as eluent with two aquagel-OH MIXED-H columns (Agilent Technologies, USA) by using a dRI detector K-2301 (Knauer, DE) and a MALS-detector MiniDAWN TREOS II (Wyatt Technologies, USA).

MALDI-TOF mass spectrometry. Matrix-assisted laser desorption/ionization time-of-flight mass spectrometry (MALDI-TOF MS) of all samples was done with an Autoflex Speed MALDI-TOF spectrometer from Bruker Daltonics GmbH, equipped with a pulsed Nd:YAG laser (355 nm, 1 kHz). A mixture of *trans*-2-[3-(4-*tert*-butylphenyl)-2-methyl-2-propenylidene]-malononitrile (DCTB) and potassium acetate were used as matrix and ion adductor, respectively. For the measurements, 1.6 μL sample solution in THF (2 g L^{-1}), 8 μL of DCTB matrix solution in THF (10 g L^{-1}), and 0.8 μL of potassium acetate solution in ethanol (1 g L^{-1}) were mixed and drop-casted on the target plate. TOF-calibration was performed using PEG reference standards.

ATR-FTIR spectroscopy. FTIR spectra of **3** and **6b** were obtained using a Vertex 80v FTIR spectrometer (Bruker) with a Golden Gate Diamond ATR unit (SPECAC) and an MCT detector. Each spectrum was recorded with 100 scans and a resolution of 4 cm^{-1}. The spectra were baseline corrected and normalized to the band intensity of the C–O asymmetric stretching vibration of PCL at 1240 cm^{-1}.

DLS. Dynamic light scattering (DLS) measurements of **6a** and **6b** were performed at 20 °C and at concentrations of 0.025 to 1 g L^{-1} in water, 2.5 to 20 g L^{-1} in acetone, 5 and 10 g L^{-1} in ethyl acetate and 10 g L^{-1} in dichloromethane using cylindrical quartz-glass cuvettes and a light scattering setup equipped with an ALV-SP125 goniometer, an ALV/LSE5004 multi tau correlator at a fiber optical ALV/High QE APD avalanche photodiode with pseudo-cross correlation and a He/Ne laser (632.8 nm, Thorlabs Inc.). The solutions were filtered prior to the measurements. The solutions in the organic solvents were used after dissolution with stirring overnight at room temperature. In contrast, the water solutions of **6b** were brought to 70 °C to completely dissolve them and then cooled back to 20 °C.

DSC. DSC experiments of **1**, **6a** and **6b** were performed with a DSC Q2000 and DSC 2500 (TA Instruments, USA). Melting and crystallization experiments were performed in water under nitrogen at a sample concentration of 20 g L^{-1} with heating and cooling rates of 10 and 5 K min^{-1}, respectively. Sample suspensions (~5 mg) were weighed in Tzero-Al-hermetic pans (hermetically sealed; pressure stable up to 3 bar) and equilibrated at 10 °C for a period of 5 min. For analysis of the first and second heating, samples were heated from 10 °C to 80 °C, cooled to 10 °C, held for 30 minutes, and then reheated to 80 °C.

TEM. TEM images of **6b** were recorded with a Libra120 (Carl Zeiss Microsopy GmbH, Oberkochen, Germany) operated at 120 kV. Images were recorded in bright field at small defocus to improve the contrast. For the measurement, 2 μL of sample solution were dripped on copper grids coated with a formvar/carbon foil. After a waiting time t (between 2 seconds and 10 minutes), the sample was blotted with filter paper to remove excess specimen not adsorbed on the grid. Afterwards, 2 μL stain solution (either 2 wt% uranyl acetate in water (UCA), or 2 wt% phosphotungstic acid in water (PTA)) were dripped on the grid and excess stain solution was blotted with a filter paper after one minute. All TEM images were taken within 48 hours after preparation of the sample solutions.

Cryo-TEM. Cryo-TEM images of **6b** were acquired using the same equipment as for the TEM measurements. 2 μL of sample solution were dropped on the holey grids (Qunatifoil type R2/2), blotted with filter paper after 5 seconds, and rapidly frozen in liquid ethane at −178 °C using a Leica GP (Grid Plunging) device (Leica Microsystems GmbH, Wetzlar, Germany). All images were recorded in bright field at −172 °C. The measurements were conducted one week after preparation of the sample solutions.

Results and discussion

Synthesis and structural analysis

The synthesis of amphiphilic tetra-PCL-*b*-PEG star block copolymers **6a** and **6b** is shown in Scheme 1. First, tetra-PCL–OH **1** was synthesized by ROP of ε-CL using pentaerythritol as initiator and $Sn(oct)_2$ as catalyst, followed by terminal group functionalization with 2-(4-nitrophenyl)-benzoxazinone-based compound **2** by esterification to give **3**. Subsequently, the 2-(4-nitrophenyl)-benzoxazinone end groups of **3** were reacted with MeO–PEG–NH_2 (**5**) of different lengths (m = 16 and 47). The synthesis results are summarized in Table 1, and the ^{1}H NMR spectra of **3**, **5b**, and **6b** are shown in Fig. 1. The desired M_n of **1** (~10 kg mol^{-1}), which forms the hydrophobic core of **6a** and **6b**, was controlled by the molar ratio of ε-CL to pentaerythritol. $M_{n,NMR}$ values of 9.3 kg mol^{-1} and 9.7 kg mol^{-1} determined by ^{1}H NMR end group analysis (see ESI Fig. S3†) agree very well with the targeted value (Table 1). Functionalization of the terminal hydroxy groups of **1** was carried out with an excess of **2** in solution. The conversion of the terminal CH_2OH group, characterized by the methylene signal at 3.64 ppm in the ^{1}H NMR spectrum of **3** (see Fig. 1c), was ≥95%.

The M_n values of **3** shown in Table 1 increased slightly compared to **1**. The somewhat reduced dispersity is probably caused by the purification steps performed after functionalization. The results clearly show that no degradation of the tetra-PCL star occurred during the modification. Fig. 1b depicts the ^{1}H NMR spectrum of MeO–PEG–NH_2 (**5b**). Absence of the methyl signal of the mesyl group at 3.08 ppm indicates a high amino functionalization of **5b**, which is calculated to be about 90% based on the intensities of the methyl ether (3.35 ppm) and the CH_2NH_2 (2.84 ppm) signals. A further issue is the perfectness of the tetra-PCL star structure. Mixtures of differently substituted pentaerythritol (**7**, **8**) were obtained by sequential conversion of pentaerythritol with lauryl chloride and compound **2** (Scheme 2). The components of these mixtures serve as model compounds for NMR spectroscopic analysis. Detailed signal assignments are given in the ESI Chapter 6 and 7.† It was found that the ^{1}H NMR spectrum of tetra-PCL–OH **1** is less suitable for quantifying structural defects caused by incomplete conversion of the pentaerythritol core. However, the different substitution patterns of the core can be well distinguished in the ^{1}H NMR spectrum of compound **3**. This becomes clear by comparison with the spectrum of mixture **8** (see Fig. 2). The signals of the species with only three PCL arms ($\mathbf{CB_3}$) could be identified (~6 mol%), while lower degrees of substitution ($\mathbf{C_2B_2}$, $\mathbf{C_3B}$) could hardly be detected and are estimated to be <1 mol%. In the ^{1}H NMR spectrum of **6b** (see Fig. 1a), the signals of the benzoxazinone terminal groups disappeared completely whereas new signals could be assigned to the newly formed linking benzamide group between the PCL core and the PEG arms. Since all benzoxazinone signals disappear in the spectrum of **6b**, it can be assumed that the benzoxazinone groups on the core also participate in the reaction with amino-terminated **5b**.

The FTIR spectra of **3** and **6b** shown in Fig. 3 also confirm the complete conversion of the terminal benzoxazinone groups. In the spectrum of **3**, the carbonyl stretching band and the C=N stretching band of the benzoxazinone group are

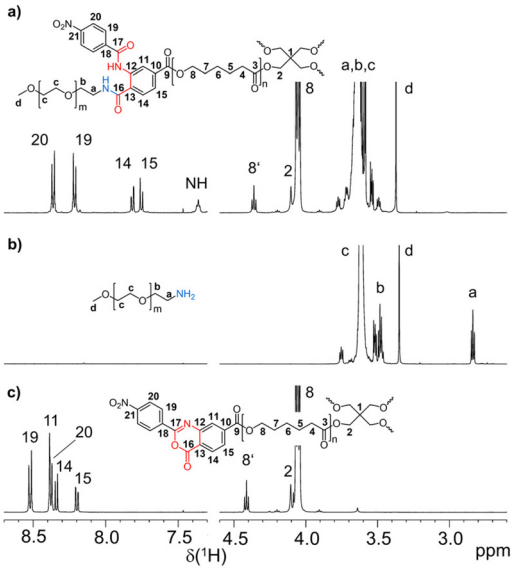

Fig. 1 ^{1}H NMR spectra (regions) of (a) tetra-PCL-*b*-PEG star block copolymer **6b**, (b) MeO–PEG–NH_2 **5b**, and (c) benzoxazinone-terminated tetra-PCL star polymer **3** (solvent: $CDCl_3$).

Table 1 Molecular characterization of **1a**, **1b**, **3a**, **3b**, **5a**, **5b**, **6a**, and **6b** by NMR spectroscopy, MALDI-TOF MS and MD-SEC measurements

Polymer	$P_{n,NMR}$ [a] (Ø $P_{n,arms} = \frac{1}{4} P_n$)	$M_{n,NMR}$ [a] (kg mol^{-1})	$M_{n,SEC}$ (kg mol^{-1})	$M_{n,MALDI\text{-}TOF}$ (kg mol^{-1})	$M_{w,SEC}$ (kg mol^{-1})	$M_{w,MALDI\text{-}TOF}$ (kg mol^{-1})	$Đ_{SEC}$	$Đ_{MALDI\text{-}TOF}$
1a	80 ± 2	9.3 ± 0.2	8.7 ± 0.6	8.6 ± 0.2	9.5 ± 0.6	8.93 ± 0.16	1.09 ± 0.3	1.04
1b	84 ± 2	9.7 ± 0.2	10.8 ± 0.6	8.9 ± 0.2	11.8 ± 0.6	9.62 ± 0.11	1.09 ± 0.2	1.09
3a	84 ± 2	10.9 ± 0.3	9.6 ± 0.7	9.7 ± 0.1	10.0 ± 0.5	10.3 ± 0.2	1.04 ± 0.3	1.06
3b	88 ± 2	11.3 ± 0.3	10.7 ± 0.5	9.5 ± 0.3	11.4 ± 0.4	9.9 ± 0.3	1.07 ± 0.2	1.04
5a	16	0.765	—	0.785	—	0.825	—	1.05
5b	47 ± 1	2.1 ± 0.1	2.1 ± 0.1	2.01 ± 0.02	2.3 ± 0.1	2.04 ± 0.02	1.06	1.02
6a	—	13.5 ± 0.3	13.9 ± 0.6	11.6 ± 0.7	15.5 ± 0.5	12.2 ± 0.7	1.11 ± 0.04	1.05
6b	—	19.3 ± 0.4	17.6 ± 0.6	16.2 ± 0.6	17.9 ± 0.6	17.1 ± 0.7	1.03 ± 0.04	1.06

[a] Based on ^{1}H NMR end group analysis (see ESI Fig. S3, S5, S7 and comments†), P_n is the degree of polymerization (number of polymer units per star).

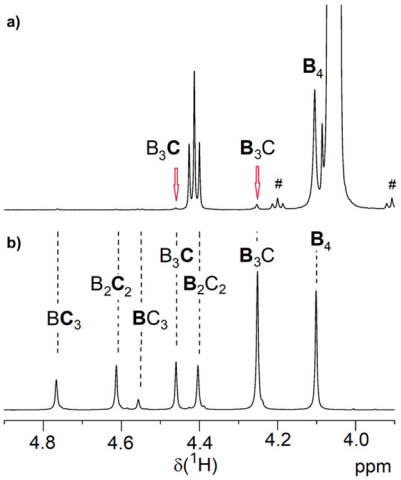

Fig. 2 Region of the ^{1}H NMR spectrum of (a) benzoxazinone-terminated star **3a** and (b) the corresponding benzoxazinone/alkyl ester-substituted compound mixture **8** (solvent: $CDCl_3$). The abbreviations are explained in Scheme 2 and symbol # marks ^{13}C satellite signals.

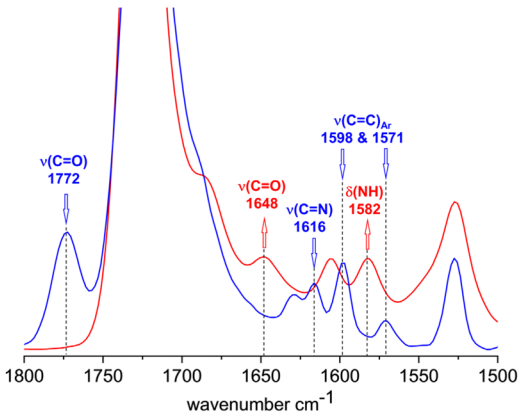

Fig. 3 FTIR spectra of **3** (blue) and **6b** (red) in the region of unreacted and reacted benzoxazinone group.

clearly visible at 1772 and 1616 cm^{-1}, respectively. After reaction with the amino-terminated PEG **5b**, these bands disappear completely in the spectrum of **6b**. Instead, amide I (carbonyl stretching band at 1648 cm^{-1}) and amide II (N–H deformation band at 1582 cm^{-1}) bands are visible, which can be attributed to the newly formed benzamide linking group.

MALDI-TOF mass spectra of **1**, **3**, **6a** and **6b** are shown in Fig. 4. To exclude mass discrimination effects, the results from the MALDI-TOF analysis were validated by measurements in linear and reflector TOF mode as well as by MD-SEC. Due to an identified slight mass discrimination for **6a**, the average molar masses of **6a**, **6b** were determined from mass spectra measured in linear TOF mode (see ESI Chapter 9†).

The spectra of tetra-PCL-star polymers **1** and **3** are well resolved and allow conclusions about the molecular architecture. This high resolution is not found in the spectra of the

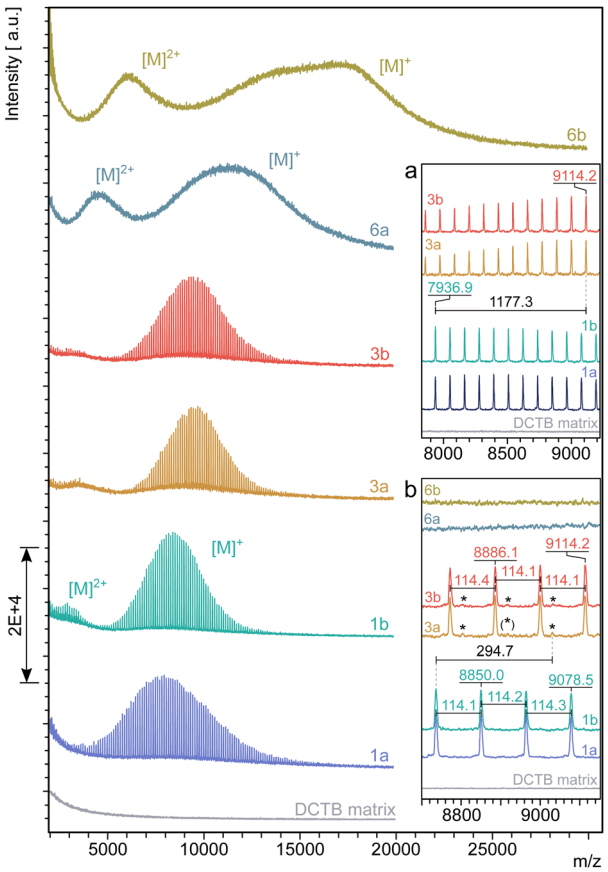

Fig. 4 Molar mass distribution determined by MALDI-TOF mass spectrometry of the star polymers **1**, **3**, **6a** and **6b** in THF with a shift in the discrete molecule masses between **1** and **3** of their main fractions by $\Delta m/z$ = 1177.3 (inset a) and the mass differences in between the discrete molecule masses $\Delta m/z$ = 114 (inset b). The most significant trace impurity found of $\Delta m/z$ = 294.7 between **1** and **3** is assigned by an asterisk.

star block copolymers **6a** and **6b** since linking of two polymers with different repeating units usually smears out the discrete signals of the individual polymers.

In the spectra of **1** and **3**, the distance between two main peaks corresponds very well to the molar mass of one repeating unit of PCL (M_n = 114.1 g mol^{-1}). The observed peak shift $\Delta m/z$ = 1177.3 between **1** and **3** (see Fig. 4a) indicates an attachment of four 2-(4-nitrophenyl)-benzoxazinone terminal units per molecule. A small, but significantly resolved trace impurity (see Fig. 4b) of $\Delta m/z$ = 294.7 may refer to a superimposition of fractions with lower number of modified terminal units ($\Delta m/z$ = 294.7 $[M + K]^+$, one unit and $\Delta m/z$ = 867.2 $[M + Na]^+$, three units). For a detailed assignment of trace impurities found by MALDI-TOF MS, see ESI Chapter 9.† The insignificantly low intensity of the mass peaks coming from trace impurities compared to the strongly dominating ones of the main fractions agrees with the findings by ^{1}H NMR spectroscopy and confirms an almost complete termination of the tetra-PCL star polymer **3** with oxazinone groups.

The molar mass measurements confirm the narrow dispersity of the samples even after the third modification step

(Table 1). There is a clear shift to higher molar masses from **1** to **3** and especially to **6a** and **6b**. The MALDI-TOF MS based molar masses tend to be slightly smaller than those determined by NMR spectroscopy and MD-SEC, but in principle show the same trend.

These results, together with the FTIR spectroscopy, MD-SEC and NMR spectroscopy measurements, show that the hetero-complementary conversion between **3** and **5** proceeded quantitatively and that the resulting star block copolymers **6a** and **6b** are characterized by high molecular uniformity.

Amphiphilic behavior in selective solvent

PCL-*b*-PEG copolymers are inherently amphiphilic because water is a selective solvent for the hydrophilic PEG block. In water, these polymers tend to form micelles,[3,15–20] whereby the micelle geometry is controlled in first instance by the volume fraction of the soluble block[33] with only small changes for a low functionality as 4 (number of arms). Since both PEG and PCL have a density close to 1.13 g cm^{-3}, the PEG volume fraction of **6a** and **6b** are approximately 23% and 44%, respectively. For linear PEG-*b*-PCL block copolymers, precipitate was found in one work below 12% PEG fraction.[34] Vesicles with sizes ranging from 60 nm to 10 μm were found[35] for compositions between 9% and 36% PEG.[34–37] Cylindrical micelles with a length up to 20 microns may form between 13% and 55% PEG.[19,34,35,37–39] Also, a lamellar phase was observed for 11% to 16% PEG[19] that could be an intermediate state of vesicle formation. The different particulate structures mentioned above overlap significantly, which complicates the analysis and a discussion of these solutions in addition to possible transitions between different morphologies that can be driven by crystallization[40] and possible concentration dependencies of the observed morphologies.[41] Similar to the linear block copolymers, we expect that sample **6a** may form a broad variety of different morphologies. This complicates a quantitative analysis of particle size by DLS. For block copolymers with a composition comparable to **6b**, most of the above mentioned works report only spherical micelles; only sometimes[38,39] cylindrical micelles are detected, see also ESI Table S4.†

The solubility of the tetra-PCL-*b*-PEG star block copolymers **6a** and **6b** in water was investigated at room temperature and at 80 °C. For this purpose, both polymers were suspended in water at a concentration of 10 mg mL^{-1} at room temperature (see Fig. 5, left). After heating to 80 °C, a clear solution of **6b** was obtained within 5 minutes (see Fig. 5, right), which remained stable when cooled back to room temperature. In contrast, **6a** remained cloudy over the entire temperature range without the formation of a precipitate (see Fig. 5, right). Both observations agree with the formation of spherical micelles in the low nm range for **6b** and the formation of micelles with a size comparable to the wavelength of light or larger for **6a**. The equilibrium melting temperature was estimated to be close to 64 °C[42,43] for PCL and around 70 °C[42–45] for PEG. Crystallization temperatures up to 49 °C[46,47] and around 40 °C[48,49] were reported for PCL and PEG, respectively. Thus, thermal treatment at 80 °C melts crystalline portions of both

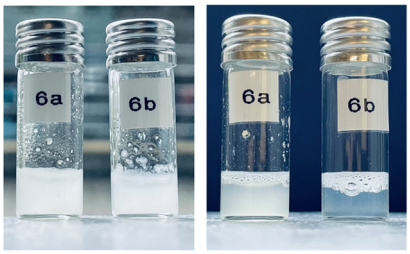

Fig. 5 Suspensions of **6a** and **6b** in water at room temperature (left) and after 5 min of heating to 80 °C and subsequent cooling to room temperature (right).

polymers, which is a mandatory step for dissolving the star block copolymers. Phase separated PCL domains may crystallize upon cooling back to room temperature. To gain a better insight into the solution and self-assembly behavior of tetra-PCL-*b*-PEG star block copolymers in water, DSC, (cryo-)TEM, DLS, and ^{1}H NMR measurements were performed on aqueous dispersions of **6a** and **6b**.

Thermal behavior in water. DSC measurements were performed on the star block copolymers **6a** and **6b** as well as on the star polymer **1** suspended in water. The DSC heating and cooling runs are shown in Fig. 6, and the results are summarized in Table 2. We take the peak position of the heat flow as rough estimates for the melting and crystallization temperature, if a peak can be observed. In the first heating run of the dispersion of **1**, a distinct melting transition is visible at about 52 °C. During cooling, crystallization appears close to 30 °C. In the second heating run, the melting is slightly shifted to lower temperatures (T_m = 46 °C), indicating a smaller stem length of the crystals. At the end of the synthesis, specimen **1** was precipitated from a concentrated CH_2Cl_2 solution into a 10-fold amount of cold methanol followed by filtration and drying in vacuum. This process determines the geometry of the PCL crystals prior to the first heating run, while the melting temperature of the second heating run is related to the stem length of the crystalline PCL domains in water.

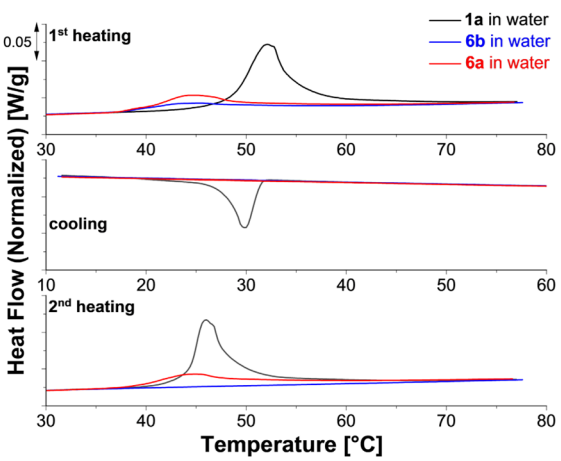

Fig. 6 DSC thermograms of **1a** (black), **6a** (red) and **6b** (blue) in water.

Table 2 Thermal behavior of **1a**, **6a** and **6b** in water

Polymer	1st heating run T_m [a] (°C)	cooling run T_c [b] (°C)	2nd heating run T_m [a] (°C)
1a	52.1	29.9	46
6a	45	—	45
6b	45	—	—

[a] Melting temperature. [b] Crystallization temperature.

Compared to **1**, the melting transitions of the star block copolymers **6a** and **6b** appear in the first heating run at lower temperature (T_m = 45 °C). This difference results in part from the different treatment of the specimens at the end of the synthesis: **6a** and **6b** are purified in water followed by freeze-drying. Thus, the crystal geometry is here affected by the micelle geometry that is established during this process. During cooling, no crystallization is visible for either copolymer. The second heating scan, recorded after 30 minutes of isothermal annealing at 10 °C, shows a melting peak only for the sample with the shorter PEG block (**6a**). For explaining this difference, we consider the visible appearance of the samples and the morphologies reported in literature, see ESI Table S4.† Based on this information, we expect mainly small spherical micelles for **6b** and larger structures possibly cylindrical micelles or vesicles for **6a**. Semi-crystalline vesicles and cylindrical micelles of PCL-*b*-PEG copolymers with a similar composition as **6a** and **6b** were analyzed previously.[34] Crystallization of vesicles was possible at room temperature, while significant crystallization of cylindrical micelles occurred only significantly below 0 °C. Our observations, therefore, hint towards a significant volume fraction of vesicles in aqueous suspensions of **6a**.

Micelle morphology: TEM and cryo-TEM. Optical techniques like TEM and cryo-TEM provide direct access to the morphology of the micelles. However, TEM requires staining and adsorption of the micelles on a substrate, which may impact the morphology of the micelles[50] or their tendency to crystallize. Cryo-TEM shows typically only the phase separated portion of the micelles. A combination of both allows to check morphological changes and to gain information about the dissolved part of the micelles. Fig. 7 shows two typical TEM micrographs where **6b** was stained with PTA (top) or with UAC (bottom). Our general observation is that PTA leads to a larger tendency of spherical micelles (a) to aggregate. Flat structures parallel to the surface develop (c) or might be initiated by cylindrical micelles that tend to appear in bundles (b). For UAC stained samples, adsorbed micelles tend to combine in larger structures, the onset of spherulitic structures is possible, and some larger flat objects with a round geometry form (d). This figure contrasts with the cryo-TEM results of Fig. 8 where we observe a large abundance of spherical micelles and only some cylindrical ones.

We argue that the structures that are visible on the TEM images but do not appear on the cryo-TEM images are most likely surface initiated with additional dependence on the particular stain. The common structure observed in all images are spherical and cylindrical micelles. The diameters of the spherical micelles were determined by manual measurement of typically 30 micelles using the Fiji software. The results are summarized in Table 3. Our data agree with literature data on linear block copolymers that are equivalent to a single arm of our star block copolymers. For instance, the PCL_{24}–PEG_{44} blocks similar to star arms produce 21.7 ± 5.9 nm sized spherical micelles[19] (stained with PTA and prepared using a different protocol) in quantitative agreement with our work (see Table 3).

The diameter of the cylindrical micelles in cryo-TEM was 12 ± 2 nm in 10 g L^{-1} samples and 13.5 ± 0.7 in 1 g L^{-1} samples. With UCA, a cylindrical micelle thickness of 21 ± 3 nm was measured in samples adsorbed from 1 g L^{-1} solution.

We now attempt to correlate the above measurements. Let us assume that the PEG corona of the micelles is not visible in

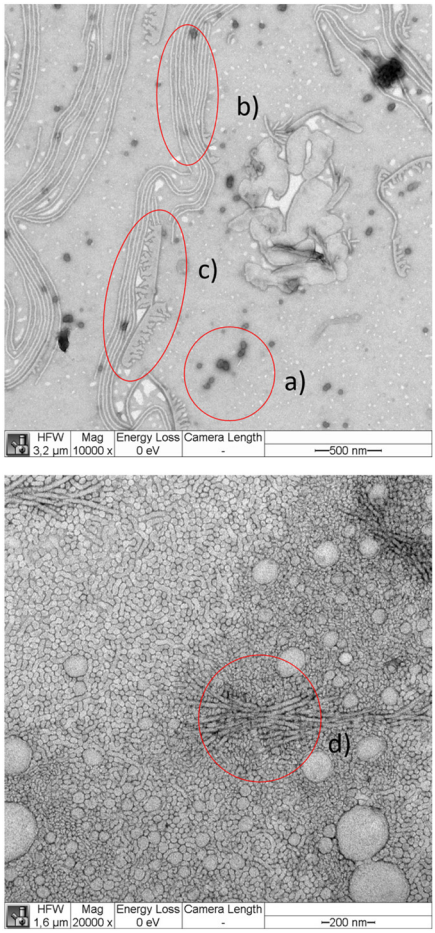

Fig. 7 TEM micrograph of **6b** adsorbed within 10 seconds from 1 g L^{-1} solution in water stained with PTA (top) and adsorbed within 10 seconds from 10 g L^{-1} solution in water stained with UAC (bottom). PTA enters predominantly the PEG corona. Thus, spherical micelles are grey objects with a darker boundary (a), cylindrical micelles as double grey lines (b), while flat surface structures have average grey color with a darker line as boundary (c). UAC stained objects show a similar appearance as PTA stained objects with characteristic super structures (d).

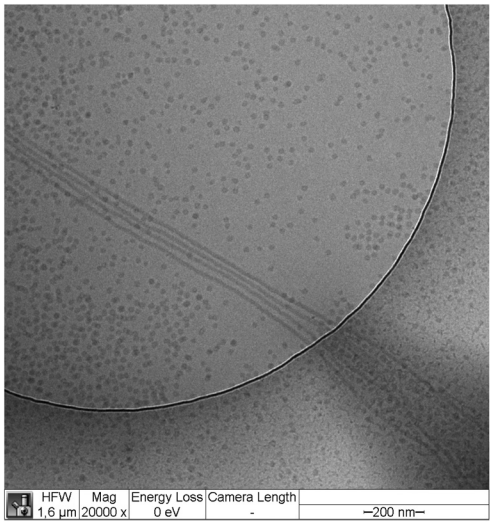

Fig. 8 Cryo-TEM image of a rapidly frozen 10 g L^{-1} solution of **6b**.

Table 3 Size of spherical micelles of **2b** in water determined by TEM with PTA or UAC as stain or by cryo-TEM

	Particle size (nm)		
Method	(0.1 g L^{-1})[a]	(1 g L^{-1})[a]	(10 g L^{-1})[a]
TEM (PTA)	28 ± 8	30 ± 5	38 ± 17
TEM (UAC)	25 ± 5	29 ± 5	24 ± 4
Cryo-TEM		15 ± 3	16 ± 3

[a] Concentration of the sample solution.

the cryo-TEM images and that the stain does not penetrate the PCL domain. Since PEG is about half of the molar mass of **6b**, dry adsorbed undeformed spherical micelles in TEM should have a size approximately $2^{1/3}$ times larger than the PCL core, *i.e.* about 20 nm, which is below the size given in Table 3. In the dry adsorbed state, the PEG tails are still swollen by the stain and may develop conformations that are either collapsed due to drying or significantly stretched, when the PEG with the stain inside tends to spread over the substrate. To understand which of these effects is more relevant, we consider Flory's characteristic ratio C_∞ of PEG that ranges roughly from 4 to 7[51] in literature with rotational isomeric state computations around C_∞ = 5.[52] For a root mean square bond length of 1.46 nm,[53] this latter estimate corresponds to a Kuhn segment size of about 8.8 Å with a Kuhn molar mass of 107 g mol^{-1}. The 2100 g mol^{-1} PEG tails of the star arms consist, therefore, of approximately 20 Kuhn segments. Assuming random walk conformations of the PEG tails as lower bound for the thickness of a PEG corona in non-stretched conformations, we estimate that this layer is at least 4 nm thick and the micelles should appear of at least 23 nm size in TEM. Fully stretched chain conformations on the substrate would lead to a layer of about 17 nm thickness leading to a maximum size of 50 nm in the adsorbed state. Our data lie in between these limits and are in accordance with a weakly stretched PEG corona in the dry adsorbed state or alternatively, a weak penetration of the stain into the PCL domain.

PCL in the crystalline state adopts almost planar zig-zag conformations deviating slightly from the fully extended form[54] with a fiber axis of 1.705 nm corresponding to two chemical monomers. Thus, A cylindrical micelle diameter of 12 ± 2 nm refers to about 13 monomers in nearly fully extended conformations. The PCL cores of **6b** contain approximately 21 monomers per arm. Thus, the diameter of the cylindrical micelle is presumably a one-folded crystal with about 11 monomers in nearly fully extended conformation. A micelle core of about 15–16 nm is almost midway between a one-folded crystal or a fully extended conformation of PCL arms, and thus, not in accord with an expected crystalline morphology.[43] Since also DSC did not show crystallization of **6b**, we conclude that the spherical micelles at room temperature consist of an amorphous PCL core.

A crystalline tetra-PCL star with $M_n \sim 10$ kg mol^{-1} and a density around 1.2 g cm^{-3},[54] occupies a volume of about 14 nm^3. A sphere with a diameter of 15–16 nm and a volume of order 2000 nm^3 provides space for roughly 140 such tetra-PCL star cores and about 1.4 nm^2 surface area per PEG tail. In comparison, thinner cylindrical micelles with 12–13 nm diameter provide only about 1.2 nm^2 per PEG tail. A similar ratio is obtained when considering amorphous PCL. This reduction refers to an energetic barrier for forming cylindrical micelles as long as the PEG remains dissolved and amorphous, indicating that spherical micelles are at least meta-stable. This barrier can be overcome, for instance, by significant changes of the solvent quality, by adjusting temperature, or when surface adsorption or favorable interactions with some solutes increase the PEG concentration locally, since the solvent quality of water decreases with the PEG volume fraction.[55,56] This may explain the lower frequency of cylindrical micelles and short precursors of these in the cryo-TEM images despite of the longer storage time of the solution prior to the measurement (7 days) as compared to the micrographs with UCA and PTA stain (up to 2 days). In consequence, we expect that solutions of **6b** immediately after heating beyond the melting temperature develop a dominant portion of spherical micelles but will not exhibit a significant portion of cylindrical micelles.

Samples **6a** in comparison to **6b** contain shorter PEG tails which stabilize these samples less against morphological changes that might be induced by contact with a surface, staining, or due to temperature changes during sample preparation. Since morphological changes were already a serious issue for **6b**, we omitted a similar analysis of **6a**.

Particle size analysis by DLS. DLS studies were first performed in different organic solvents with the aim of identifying good solvents for both PEG and PCL. Prior to the measurements, we scanned literature to identify possible solvents, see ESI Section 10, Table S5.† Tetrahydrofuran, toluene and chloroform were analyzed in our preceding paper.[23] In the present work, we employ acetone, ethyl acetate, and dichloro-

methane at different concentrations between 2.5 and 20 g L^{-1}. The R_H values of **6b** determined from the DLS measurements are summarized in the ESI Table S1.† The distribution of R_H is monodisperse in dichloromethane and ethyl acetate. At 10 g L^{-1}, we obtain 3.8 ± 0.3 and 4.3 ± 0.1 nm, respectively. For comparison, an estimate of R_H by computing R_g with C_∞ = 5 and a Kuhn segment size of about 9 Å for PCL[32] and the parameters for PEG mentioned above yields R_H = 3.4 when using R_g/R_H = 1.05 for experimental data.[57] Therefore, these solvents are presumably good solvents for the polymers. Surprisingly, our data indicate that ethyl acetate is the better solvent for the copolymer, which contrasts the trend expected from literature data, see ESI Section 10, Table S1.† In acetone, the data fit is best when a bidisperse particle distribution is assumed, see ESI Fig. S1.† The fast mode yields a hydrodynamic radius of R_H = 3.0–3.6 nm for **6a** and R_H = 3.6–4.2 nm for **6b** depending on the concentration. The latter is in good agreement with the hydrodynamic radius in dichloromethane and ethyl acetate indicating dissolved single star block copolymers in the sample. The reduced size of **6a** compared to **6b** reflects the lower molar mass of this compound.

The slow mode refers to a hydrodynamic radius that increases with concentration between 14–23 nm and 18–34 nm in the case of **6a** and **6b**, respectively, see ESI Table S1.† Such a behavior is typically attributed to the formation of aggregates or clusters. The nature of these clusters, however, remains unclear: literature data for the solvent quality of acetone regarding both PEG and PCL is scattered around the theta condition, see ESI Table S5.† Furthermore, the relative amplitude of the fast component in the ESI Table S1† does not strongly decay with concentration as one expects for micelle formation or other forms of associations where increasing concentrations favors associations.

For analyzing **6b** in water, samples were prepared at 20 g L^{-1}, heated up to 70 °C and cooled back to room temperature. Afterwards, the solution was diluted stepwise to a lowest concentration of 0.025 g L^{-1}. All measurements were conducted within 6 h after preparation starting from the largest concentration. In all samples, monodisperse clusters with a hydrodynamic radius of 20–22 nm are observed, see ESI Table S1.† The size of the dried adsorbed stained micelles in TEM is about 10 to 15 nm less than the particle diameter measured by DLS, which is reasonable when considering the swelling of the densely grafted PEG tails in water, a possible weak penetration of the stain into the PCL, and additional corrections like a weak dispersity of the PEG tails. Up to the end of our measurement time of 6 h, we detect no significant traces of larger species like cylindrical micelles of sample **6b** in water.

Temperature-dependent ^{1}H NMR measurements in water. Variable temperature (VT) ^{1}H NMR measurements were performed on suspensions of star block copolymers **6a** and **6b** in D_2O to investigate the influence of the different PEG block length at constant PCL core size on the molecular dynamics (see Fig. 9 and ESI Fig. S19 and S20†). The standard high-resolution NMR measurements performed here require sufficient mobility of the structural units accompanied with long T_2 relaxation times to detect the corresponding NMR signals. This qualitative study is based on the detection of mobility changes during heating from 30 to 80 °C. For both samples, the PCL signals are collapsed at 30 °C, and only for **6b** a broadened ^{1}H NMR signal at ~3.65 ppm indicates PEG mobility. With increasing temperature, the changes for both samples are quite different. From ~45 °C, broad signals appear for both the PCL and PEG moiety of **6a** that steadily increase in intensity with further increase in temperature but remain broad (see Fig. 9b and ESI Fig. S19†). For **6b**, a steep increase in intensity of all signals is observed in the narrow temperature range from ~35 °C to ~45 °C with only minor changes at higher temperatures (see Fig. 9a and ESI Fig. S20†). Spectra recorded at 40 °C over a period of one hour are identical and indicate a steady state at a given temperature (see ESI Fig. S21†). Within this temperature range the turbid sample becomes clear and remains so, while the sample of **6a** remains turbid over the whole range studied. The behavior of the two samples also differ when they are cooled back to 30 °C (see Fig. 9c and d). For **6a**, the signals start to broaden with cooling and after keeping the sample at 30 °C for one hour, the residual signals disappear (see Fig. 9d and ESI Fig. S19†). Comparison with the spectrum of the initial sample at 30 °C (see Fig. 9b) shows that the sample has returned to its original state. A comparable behavior is observed for a dispersion of the unmodified and water-insoluble PCL core **1b** (see ESI Fig. S22†). The spectrum of **6b** after cooling to 30 °C (see

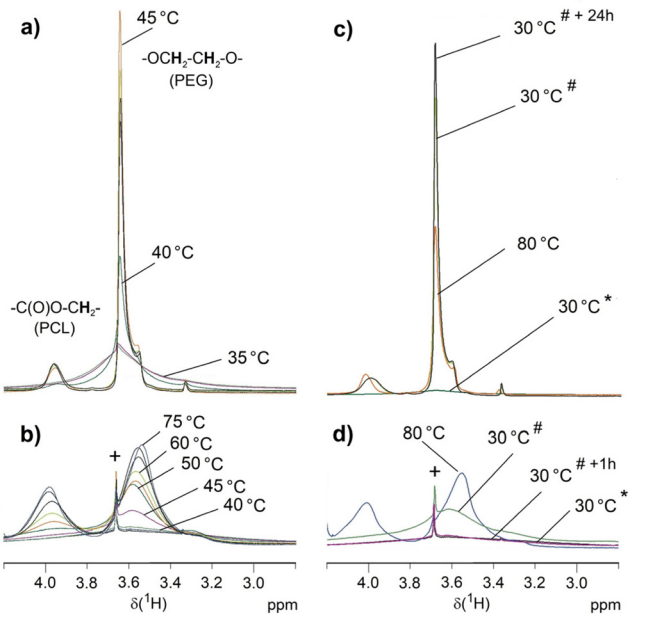

Fig. 9 VT ^{1}H NMR measurements on **6b** (a and c) and **6a** (b and d) in D_2O (suspension of 5 g L^{-1}). Only selected temperatures are indicated. The complete series are depicted in the ESI Fig. S19 and S20.† Besides the initial spectra at 30 °C (*), (c) and (d) show additional spectra recorded after cooling down the samples to 30 °C (#) and after keeping the sample for one hour (**6a**) or 24 hours (**6b**) at 30 °C (*+1 h, *+24 h). Symbol + marks the signal of a trace of unreacted **5** that is the only compound dissolved at 30 °C.

Fig. 9c) resembles almost the high-temperature spectrum and remains unchanged within 24 hours. The PCL/PEG ratio determined for **6b** from the ^{1}H NMR spectra at 80 °C and at 30 °C (24 h) matches the ratio determined in $CDCl_3$ as a good solvent. Also, for **6a** the PCL/PEG ratio at 80 °C is very similar to that of the $CDCl_3$ solution.

The findings of these VT ^{1}H NMR experiments correspond to the results of crystallization studies in water by DSC and to the DLS results. The PCL phase of the dispersed samples prior to the first heating is a rigid phase and therefore the spectrum is silent for these signals. The PEG chains are also immobile and only the outermost PEG sphere of **6b** seems to show a mobility sufficient to detect a signal. At the melting range of the PCL core ($T_m \sim 45$ °C, see Table 3) the corresponding signals appear for both star block copolymers, which is associated with increased mobility. This is confirmed by a reference experiment on the water-insoluble PCL core **1a** that also shows resolved signals above T_m. The PEG chains become also more mobile but only for **6b** the PEG signal is narrow with a hump probably indicating a still ordered PEG portion. For **6b**, micellar structures form in this process, which have high stability. This agrees with the DLS measurements that after heating the sample to 70 °C and subsequent cooling prove stable micellar structures with hydrodynamic radii of about 20 nm at 25 °C for **6b**. PCL recrystallization is suppressed in the micellar structures and the ^{1}H NMR signals of PCL remain unchanged after cooling. The two blocks are mobile enough in their entirety in these micellar structures to be quantitatively detected by solution-state NMR techniques as confirmed by the PCL/PEG ratio, which is consistent with that of the $CDCl_3$ solution. The linking groups between both blocks result in well-resolved signals in accordance to the mobility of both blocks. For **6a**, the mobility of the short PEG chains seems to be hindered by the larger PCL fraction as indicated by the rather broad signal also at 85 °C. However, the mobility in both blocks is sufficient to largely reflect the PCL/PEG ratio from the $CDCl_3$ solution in the signal integrals and also the signals of the linking groups can be detected. Different to **6b**, the increased mobility within the particles during heating does not result in the formation of small micellar structures with a size below the wavelength of visible light in the aqueous environment. Below T_m of PCL, re-formation of a largely immobilized structure occurs, leading to signal collapse for both PCL and PEG in these high-resolution NMR measurements.

In conclusion, these straightforward ^{1}H NMR experiments on suspensions in D_2O allow a qualitative evaluation of melting and recrystallization as well as micellar structure formation for these tetra-PCL-*b*-PEG star block copolymers as demonstrated here for the influence of different PEG chain lengths. The increase in mobility with temperature should be due to both melting PCL structures and solvation of the hydrophilic PEG chains. The formation of small cylindrical micelles or spheres requires a sufficiently high content of the hydrophilic PEG as obviously realized for **6b** but not for **6a**.

Conclusions

In this work, a combination of "core fist" and "grafting-onto" approach was presented to prepare two uniform tetra-PCL-*b*-PEG star block copolymers with PCL cores of the same size but with PEG arms of different lengths. The synthesis was carried out by reacting a benzoxazinone-terminated tetra-PCL star with amino-terminated linear PEG. The polymers are characterized by a high degree of uniformity, which can be attributed to the use of structurally uniform starting components and to the quantitative conversion of the reacting end groups. Comprehensive studies of the synthesized star polymers by NMR and ATR-FTIR spectroscopy confirmed the quantitative conversion of the benzoxazinone-terminated tetra-PCL star polymer with the amino-terminated linear PEG chains. The expected molar masses as well as their uniformity were confirmed by MD-SEC measurements and MALDI-TOF MS. In addition, DSC, DLS and ^{1}H NMR measurements in the selective solvent water provided insights into the amphiphilic character. After heating suspensions of the star block copolymers in water above the melting point of PCL (T_m = 45 °C), only the star block copolymer with m = 47 repeating units of PEG and n = 22 repeating units of PCL per arm formed a clear solution with spherical micellar structures in a wide concentration range. The suspension of the star block copolymer with m = 16 and n = 21 in water remained cloudy after heating above T_m. Here large structures form, presumably vesicles that allow recrystallization of the PCL cores upon cooling. DLS measurements of aqueous solutions of the larger star polymer within 6 hours after preparation indicate no formation of cylindrical vesicles. Cryo-TEM images show the formation of some cylindrical micelles after 6 days. This indicates that the spherical micelles are likely a metastable state where the samples lock in during cooling. The studies show that the length of the PEG chains can be used to tune size, stability, and crystallinity of micelles made of star block copolymers in water.

With regard to the self-assembly behavior of the star block copolymers, the question arises as to the influence of the relatively large benzoxazinone linker group. In particular, the strong electron-withdrawing effect of the nitro group suggests the formation of strong dipole–dipole interactions at this structural unit. This type of interaction is also thought to occur in the synthesis of related amphiphilic networks and to be responsible for specific deviations in the network connectivities.[23] This is the subject of further investigation using various spectroscopic methods directed at the specific interactions of these groups with each other and with the solvents used. In the case of the star polymers studied here, it is expected that in polar solvents such as water the dipole–dipole interactions are suppressed, so that the remaining hydrophobic interactions of the linker groups predominate. The extent to which this influences the association behavior of the star block copolymers in water or other solvents cannot be conclusively clarified from the present studies. Comparative studies with alternative linker groups are planned for this purpose.

Conflicts of interest

There are no conflicts to declare.

Acknowledgements

This work was performed within the collaborative research project "Adaptive polymer gels with model network structure" (FOR2811), funded by the German Research Foundation (DFG), grant numbers 397384169, 423514254, 423478088 and 423373052. We thank Christina Harnisch and Alissa Seifert (IPF Dresden) for SEC measurements. Differential scanning calorimetry experiments were performed by Kerstin Arnold and ATR-FTIR spectroscopy measurements was done by Dr Mikhail Malanin.

References

1 Y. Zhang, T. Guan, G. Han, T. Guo and W. Zhang, *Macromolecules*, 2019, **52**, 718–728.
2 A. S. R. Oliveira, P. V. Mendonça, S. Simões, A. C. Serra and J. F. J. Coelho, *J. Polym. Sci.*, 2021, **59**, 211–229.
3 P. Dong, X. Wang, Y. Gu, Y. Wang, Y. Wang, C. Gong, F. Luo, G. Guo, X. Zhao, Y. Wei and Z. Qian, *Colloids Surf., A*, 2010, **358**, 128–134.
4 K. Ishizu and S. Uchida, *Prog. Polym. Sci.*, 1999, **24**, 1439–1480.
5 W. Burchard, in *Branched polymers II*, Springer, 1999, pp. 113–194.
6 A. J. Inglis, P. Pierrat, T. Muller, S. Bräse and C. Barner-Kowollik, *Soft Matter*, 2010, **6**, 82–84.
7 A. M. Bhayo, R. Abdul-Karim, S. G. Musharraf and M. I. Malik, *RSC Adv.*, 2018, **8**, 28569–28580.
8 T. Öztürk, A. Kiliçlioğlu, B. Savaş and B. Hazer, *J. Macromol. Sci., Part A: Pure Appl.Chem.*, 2018, **55**, 588–594.
9 A. Imdad, K. Faheem, R. Sana, P. Samina, A. Shakil, S. Muhammad Raza and M. Muhammad Imran, *React. Funct. Polym.*, 2020, **150**, 104553.
10 X. Yan, J. Li and T. Ren, *RSC Adv.*, 2018, **8**, 29464–29475.
11 Ö. Gökçe Kocabay and O. İsmail, *Int. J. Polym. Mater. Polym. Biomater.*, 2021, **70**, 328–337.
12 A. Behl, V. S. Parmar, S. Malhotra and A. K. Chhillar, *Polymer*, 2020, **207**, 122901.
13 H. Chunyan, C. Zhuo, W. Shengjie, H. Yanfeng, W. Hai, S. Hongfan, K. Deling, L. Xigang, W. Chun, Z. Linhua and Z. Dunwan, *Chin. Chem. Lett.*, 2017, **28**, 1905–1909.
14 K. S. Shalaby, M. E. Soliman, G. Bonacucina, M. Cespi, G. F. Palmieri, O. A. Sammour, A. A. El Shamy, L. Illum and L. Casettari, *Pharm. Res.*, 2016, **33**, 2010–2024.
15 C. Lu, S.-R. Guo, Y. Zhang and M. Yin, *Polym. Int.*, 2006, **55**, 694–700.
16 C. Lu, L. Liu, S.-R. Guo, Y. Zhang, Z. Li and J. Gu, *Eur. Polym. J.*, 2007, **43**, 1857–1865.
17 S. Guo and Y. Zhang, *J. Polym. Sci., Part B: Polym. Phys.*, 2008, **46**, 1412–1418.
18 Z.-X. Du, J.-T. Xu and Z.-Q. Fan, *Macromol. Rapid Commun.*, 2008, **29**, 467–471.
19 Z.-X. Du, J.-T. Xu and Z.-Q. Fan, *Macromolecules*, 2007, **40**, 7633–7637.
20 J. J. Crassous, P. Schurtenberger, M. Ballauff and A. M. Mihut, *Polymer*, 2015, **62**, A1–A13.
21 M. Alami-Milani, P. Zakeri-Milani, H. Valizadeh, R. Salehi and M. Jelvehgari, *Iran. J. Basic Med. Sci.*, 2018, **21**, 153.
22 N. Brigham, C. Nardi, A. Carandang, K. Allen and R. M. Van Horn, *Macromolecules*, 2017, **50**, 8996–9007.
23 C. Bunk, L. Löser, N. Fribiczer, H. Komber, L. Jakisch, R. Scholz, B. Voit, S. Seiffert, K. Saalwächter, M. Lang and F. Böhme, *Macromolecules*, 2022, **55**, 6573–6589.
24 M. Lang, R. Scholz, L. Löser, C. Bunk, N. Fribiczer, S. Seiffert, F. Böhme and K. Saalwächter, *Macromolecules*, 2022, **55**, 5997–6014.
25 K. Hagmann, C. Bunk, F. Böhme and R. von Klitzing, *Polymers*, 2022, **14**, 2555.
26 L. Jakisch, M. Garaleh, M. Schäfer, A. Mordvinkin, K. Saalwächter and F. Böhme, *Macromol. Chem. Phys.*, 2018, **219**, 1700327.
27 H. Zhang, L. Jakisch, H. Komber, B. Voit and F. Böhme, *Tetrahedron*, 2013, **69**, 3656–3663.
28 L. Jakisch, H. Komber and F. Böhme, *Macromol. Mater. Eng.*, 2007, **292**, 557–570.
29 L. Jakisch, H. Komber and F. Böhme, *J. Polym. Sci., Part A: Polym. Chem.*, 2003, **41**, 655–667.
30 S. Ishii, H. Kokubo, K. Hashimoto, S. Imaizumi and M. Watanabe, *Macromolecules*, 2017, **50**, 2906–2915.
31 K. A. Barrera-Rivera, R. Vera-Graziano, E. López-Sánchez and A. Martinez-Richa, *J. Polym. Res.*, 2015, **22**, 1–8.
32 Y. Huang, Z. Xu, Y. Huang, D. Ma, J. Yang and J. W. Mays, *Int. J. Polym. Anal. Charact.*, 2003, **8**, 383–394.
33 S. Jain and F. S. Bates, *Science*, 2003, **300**, 460–464.
34 K. Rajagopal, A. Mahmud, D. A. Christian, J. D. Pajerowski, A. E. Brown, S. M. Loverde and D. E. Discher, *Macromolecules*, 2010, **43**, 9736–9746.
35 J. A. Zupancich, F. S. Bates and M. A. Hillmyer, *Macromolecules*, 2006, **39**, 4286–4288.
36 P. P. Ghoroghchian, G. Li, D. H. Levine, K. P. Davis, F. S. Bates, D. A. Hammer and M. J. Therien, *Macromolecules*, 2006, **39**, 1673.
37 J. Zhou, R. Ni and Y. Chau, *RSC Adv.*, 2017, **7**, 17997–18000.
38 Y. Geng and D. E. Discher, *J. Am. Chem. Soc.*, 2005, **127**, 12780–12781.
39 J.-X. Yang, B. Fan, J.-H. Li, J.-T. Xu, B.-Y. Du and Z.-Q. Fan, *Macromolecules*, 2016, **49**, 367–372.
40 A. M. Mihut, J. J. Crassous, H. Schmalz, M. Drechsler and M. Ballauff, *Soft Matter*, 2012, **8**, 3163–3173.
41 N. Fairley, B. Hoang and C. Allen, *Biomacromolecules*, 2008, **9**, 2283–2291.
42 B. Bogdanov, A. Vidts, E. Schacht and H. Berghmans, *Macromolecules*, 1999, **32**, 726–731.

43 B. Wunderlich, *Macromolecular physics volume 3 Crystal Melting*, Academic Press, New York, 2012.
44 C. P. Buckley and A. J. Kovacs, *Colloid Polym. Sci.*, 1976, **254**, 695–715.
45 C. Luo, W. Chen and Y. Gao, *Polym. Sci., Ser. A*, 2016, **58**, 196–205.
46 P. M. Remiro, M. M. Cortazar, M. E. Calahorra and M. M. Calafel, *Macromol. Chem. Phys.*, 2001, **202**, 1077–1088.
47 R. De Juana and M. Cortazar, *Macromolecules*, 1993, **26**, 1170–1176.
48 B. Bogdanov, A. Vidts, A. Van Den Buicke, R. Verbeeck and E. Schacht, *Polymer*, 1998, **39**, 1631–1636.
49 P. C. Ashman and C. Booth, *Polymer*, 1975, **16**, 889–896.
50 P. K. Kilpatrick, W. G. Miller and Y. Talmon, *J. Colloid Interface Sci.*, 1985, **107**, 146–158.
51 G. D. Smith, D. Y. Yoon, R. L. Jaffe, R. H. Colby, R. Krishnamoorti and L. J. Fetters, *Macromolecules*, 1996, **29**, 3462–3469.
52 G. D. Smith, D. Y. Yoon and R. L. Jaffe, *Macromolecules*, 1993, **26**, 5213–5218.
53 H. Lee, R. M. Venable, A. D. MacKerell and R. W. Pastor, *Biophys. J.*, 2008, **95**, 1590–1599.
54 Y. Chatani, Y. Okita, H. Tadokoro and Y. Yamashita, *Polym. J.*, 1970, **1**, 555–562.
55 L. Huang and K. Nishinari, *J. Polym. Sci., Part B: Polym. Phys.*, 2001, **39**, 496–506.
56 W. D. Mkandawire and S. T. Milner, *Macromolecules*, 2021, **54**, 3613–3619.
57 M. Rubinstein and R. H. Colby, *Polymer physics*, Oxford university press, New York, 2003.